An Analysis of the Effect of Phosphorylation of TRIP13 at Y56 on Irradiation Resistance in Vivo

Abstract

Head and neck squamous cell carcinomas (HNSCCs) are an aggressive cancer with poor survival rates. A considerable hindrance to the successful treatment and prevention of recurrence of these cancers is the development of radiation resistance via efficient repair of DNA double strand breaks. Previous studies have found that thyroid hormone receptor interactor 13 (TRIP13) plays a role in the development of this radiation resistance, but the definitive mechanism remains unknown, and thus, effective treatments that are immune to radiation resistance are not being used clinically. In this analysis, we investigate the role of phosphorylation of TRIP13 at tyrosine 56 (Y56) in this resistance. Our data originates from a study of 9 athymic mice, 4 of which were injected with Y56F cell lines, preventing phosphorylation of Y56, and 5 of which were injected with TRIP13 cell lines, allowing for the phosphorylation of Y56. Irradiation was performed on half of each mouse and tumor volume measurements were taken. Using a linear mixed effects model with random intercepts and slopes, we find a significant difference in log tumor volume ratio (β= 0.34, p-value = 0.002), our main outcome of interest, in mice injected with cells suppressing the phosphorylation of Y56 after irradiation, leading us to conclude that phosphorylation of Y56 is required for radiation resistance in vivo. Our results imply that radiation treatments for HNSCCs should include the suppression of Y56, but further studies are needed to generalize these results to humans.

Introduction

Approximately 90% of all head and neck cancers can be attributed to a type of malignancy known as head and neck squamous cell carcinomas (HNSCCs), which develop from

the mucosal epithelium in the oral cavity, pharynx and larynx (Johnson et al., 2020). HNSCCs are the 6th most common type of cancer worldwide, with 890,000 new cases in 2018, and have poor survival rates, with almost 50% of HNSCC patients dying within 5 years (Johnson et al., 2020). Advanced HNSCC is typically treated multimodally with radiation and chemotherapy, but radiation resistance has proven to be an impediment to successful treatment.

It has been shown that thyroid hormone receptor interactor 13 (TRIP13) is highly expressed in head and neck cancers and promotes double strand repair of DNA via non-homologous end joining (Banerjee et al., 2022). Because radiation combats cancer cells by inducing double strand breaks in DNA, the efficient repair of these cells leads to radiation resistance, cancer cell survival, and thus, treatment failure. However, the precise mechanism of radiation resistance propagated by TRIP13 remains uninvestigated. When looking at potential phosphorylation sites in TRIP13, there are 3 places of potential interest: positions 56, 152, and 206. In this analysis, we focus our efforts on determining the importance of tyrosine 56 in the development of radiation resistance. We aim to determine if phosphorylation at Y56 is required for radiation resistance to HNSCC in vivo.

Methods

Study Design

To elucidate the impact of phosphorylation at tyrosine 56 on the development of radiation resistance in vivo, 9 athymic mice were injected bilaterally with squamous cell carcinoma cell lines (n = 5 mice with UM- SCC-1-Y56F and n = 4 with UM-SCC-1-TRIP13). Tumor volume was measured at least three times a week across 3-4 weeks for a total of 218 measurements. Once tumor volume reached ~100-150 mm^3, unilateral irradiation (2 Gy/day, 5

days) in both groups was performed. Volume measurements continued until the mice were euthanized.

Statistical Methods

We use trajectory plots to visualize tumor volumes over time. We fit a linear mixed effects model with knot terms at the start of each group's radiation treatment to quantify the impact of phosphorylation at Y56 on radiation resistance. We refer to the mice who received UM-SCC-1-Y56F injections, or in other words, those in which phosphorylation at Y56 is suppressed, as the Y56F group and those who received UM-SCC-1-TRIP13 injections as the TRIP13 group. To account for correlation among tumors grown in the same mouse, we use the ratio of non-irradiated tumor volume to irradiated tumor volume as our primary outcome in all models. We perform a natural logarithmic transformation on this ratio of volumes, after adding an arbitrary small value to both values, to account for exponential trends in tumor growth. Model selection of mean structures and random effect structures is performed using Likelihood Ratio Tests and by comparing Akaike Information Criteria based on models fit with maximum likelihood (ML). Model diagnostics are then performed on our final model, fit with restricted maximum likelihood (REML), to assess model fit and validity. Because we observe some abnormal measurements in one particular mouse, sensitivity analyses are performed to determine if our model is robust to influential points. All calculations are performed in R Studio Version 1.4.1717.

Results

Individual trajectories of each mouse's tumors are given in Figure 1. We see an overall upward trend in tumor volume of TRIP13 mice, indicating steady tumor growth regardless of

irradiation. Contrastingly, we see a time-invariant upward trend in only Y56 mice tumors that were not irradiated. The trend of Y56F tumor growth treated with irradiation diverts downward about half way through data collection. This impact of phosphorylation at Y56 is further emphasized by the loess smoothed curves of tumor volume over time per group and by treatment status, as shown in Figure 2. The trajectory of the smoothed curve for the Y56 tumors that received irradiation treatment changes subsequent to the start of treatment, indicating successful tumor reduction post-irradiation in this group of mice.

We model our primary outcome of interest, the log of the ratio of irradiated tumor volume to radiated tumor volume, using a linear mixed effects model. Knot terms are added for each group to account for the expected change in tumor growth after the start of irradiation treatment. We include both a random intercept and a random slope for time, as we see different baseline volumes and different growth trajectories for each tumor in Figure 1. A Likelihood Ratio Test comparing a random intercept-only model and a model with both random intercept and random slope confirms that a model with both random effects fits the data better (χ^2=32.5, p-value <0.0001). This model equation is given in Supplement 1, labeled as Equation 1. Parameter estimates and their confidence intervals for this model are provided in Figure 3.

Notably, we find a significant difference in the change in tumor volume ratio in Y56 mice before and after radiation, providing evidence that phosphorylation of TRIP13 at Y56 is required for, or at least significantly associated with, developing radiation resistance in vivo (β= 0.34, p-value = 0.002). We can interpret the model coefficients as the percent change in non-irradiated tumor volume compared to irradiated tumor volume for each group both pre- and post- start of irradiation treatment by exponentiating the coefficients and subtracting 1. For mice in the Y56

group after irradiation starts, there is a 9.12% increase, on average, in non-irradiated tumor volume when compared to irradiated tumor volume. Note that an increase in non-irradiated tumor volume when compared to irradiated tumor volume indicates successful tumor reduction via irradiation, and thus, prevention of radiation resistance development. From this, we infer that Y56 mice are responding well to irradiation treatment, but the TRIP13 mice are not.

The impact of phosphorylation of TRIP13 at Y56 on radiation resistance in vivo is further depicted in Figure 4 by the loess smoothed curves of our model outcome, the log ratio of tumor volumes, over time. We see that trends in tumor ratio over time are highly influenced by measurements of two mice, both of which are excluded in the plot on the right. From this trajectory plot, we see that for the Y56 mice, after irradiation begins, the irradiated tumor is consistently smaller than the non-irradiated tumor, endorsing the conclusions drawn earlier based on the model parameters.

We estimate our random effects via best linear unbiased prediction (BLUP) and visualize our model's predicted log volume ratio over time for each mouse by plotting the predicted and observed trajectories, as seen in Figure 5. We see that the predicted trajectories of the log volume ratio for all Y56 mice, except for the mouse with id 9, have positive slopes after the start of irradiation. Hence, our model predicts that irradiated tumor volume is smaller than the non-irradiated tumor volume for all mice in the Y56 group, except for mouse 9.

We can explain this deviation from trend in mouse 9 because this mouse has tumor volume measurements of 0 mm^3 after having non-zero volume measurements. Because we deem this to be an anomaly that is not due to irradiation treatment or group, but because of

lab error, we refit our model without data from this subject. Parameter estimates and their confidence intervals for the model without mouse 9 is given in Supplement 2. The coefficient for the interaction between day and Y56F group status changes by 22.92%, and consequently, we do not consider our model to be robust to this influential point. Markedly, using the parameter estimates from the model fit without mouse 9, we see that mice in the Y56 group have an average 17.38% increase in non-irradiated tumor volume when compared to irradiated tumor volume, a greater percent change than that of the model including mouse 9. Hence, when excluding mouse 9 from our analyses, we see a greater average impact of irradiation on Y56F mice.

To assess homogeneity of variance, we examine plots of residuals vs. fitted values for both the model with and without mouse 9. Visualizing this plot using all mice, we see some outlying points from one particular mouse, but overall no concerning trends indicating violation of this assumption (Supplement 3). We then assess normality of our models' residuals and random effects. The residuals from both models deviate from normality at the tails, indicating that this assumption is not satisfied regardless of the inclusion of data from mouse 9 (Supplement 4). Quantile-quantile (QQ) plots of our models' random intercepts and slopes show slight deviations from normality, but are not of concern to the validity of our model (Supplement 5). We do, however, see an improvement in these QQ plots when removing mouse 9 (Supplement 5).

Conclusion

In summary, we found that suppression of phosphorylation of TRIP13 at Y56 is associated with increased radiation efficacy. We used a linear mixed effects model to model the

log of the ratio of non-irradiated tumor volume to irradiated tumor volume. We included two knot terms to represent the predicted change in time slope after irradiation began for each group, as each group of mice began irradiation at different times. We found a significant difference in the change in volume ratio in Y56 mice before and after irradiation, indicating that Y56 plays an important role in the development of irradiation resistance.

It is important to note the limitations of the generalizability and utility of these results. As demonstrated by the QQ plots of residuals in Supplement 3, the error term of our model cannot be assumed to be Normally distributed. Furthermore, based on our sensitivity analysis, our model is not robust to the influential points of mouse 9. In addition, our study's small sample size impedes the power of our analyses, and thus the generalizability of our results. However, we are reassured by the fact that the predicted trajectories of the mice in our study are similar within each group. Lastly, because all data was collected in vivo, we cannot draw conclusions about the importance of Y56 in the development of radiation resistance in human HNSCCs. In future studies, we hope these results are used to investigate the suppression of Y56 in irradiation resistance in humans, and thus, to develop more effective treatments for clinical use.

Figures

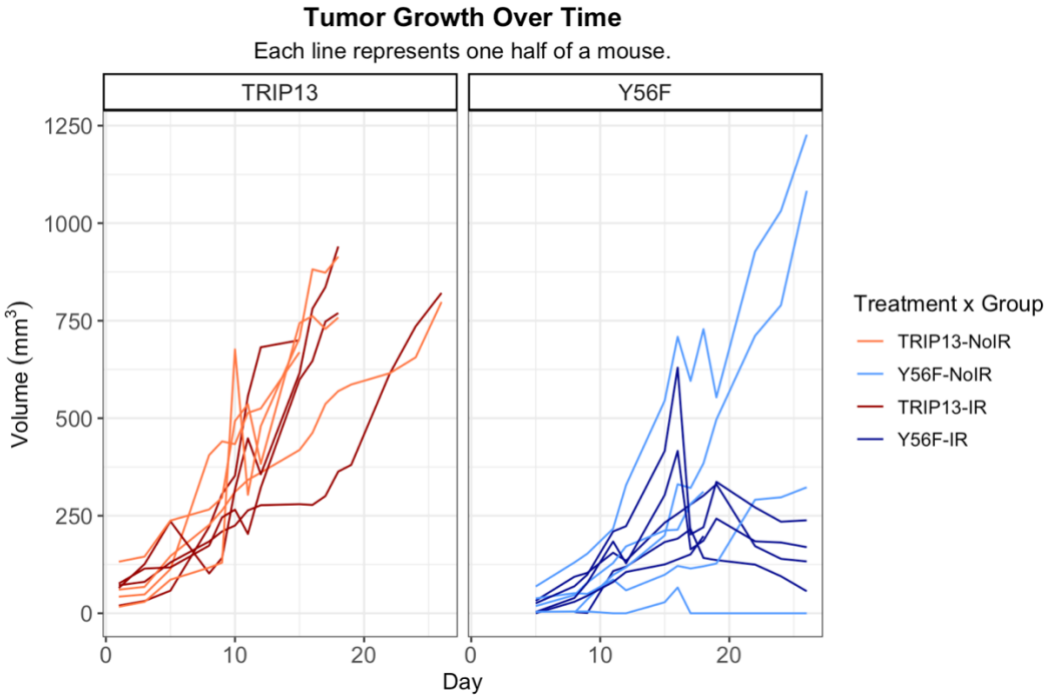

Figure 1: Individual trajectories of each tumor, faceted by group and colored by radiation treatment. As each mouse was injected with two tumors, each trajectory represents one half of a mouse.

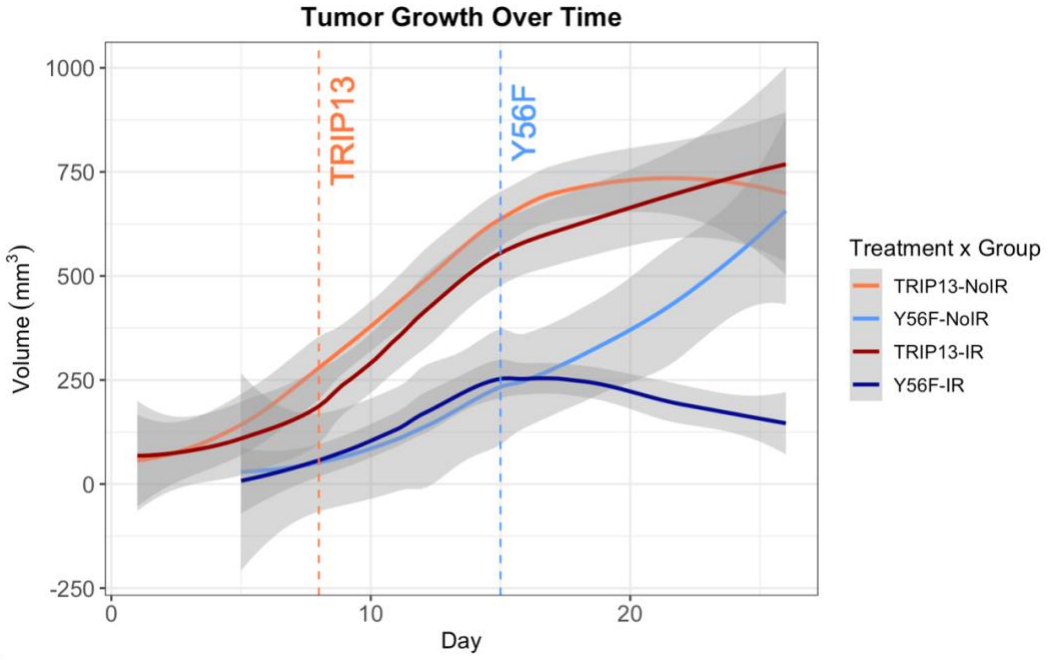

Figure 2: Loess curves of tumor volume in mm^3 over time, colored by group assignment and radiation treatment. Start of radiation for each group is indicated via dashed vertical lines. Gray shaded regions represent the 95% confidence interval of each smoothed curve.

	Log Volume Ratio		
Predictors	*Estimates*	*CI*	*p*
Day	0.08	-0.17 – 0.32	0.541
Y56F Group	2.45	-0.20 – 5.09	0.065
TRIP13 Knot	-0.11	-0.38 – 0.16	0.415
Y56F Knot	0.34	0.13 – 0.56	**0.002**
Day * Y56F Group	-0.33	-0.64 – -0.02	**0.038**
Random Effects			
σ^2	1.74		
$\tau_{00\ id}$	0.74		
$\tau_{11\ id.Time}$	0.03		
$\varrho_{01\ id}$	-0.11		
ICC	0.77		
$N_{\ id}$	9		
Observations	109		
Marginal R^2 / Conditional R^2	0.061 / 0.788		

Figure 3: Parameter estimates of the linear mixed effects model, fit with REML.

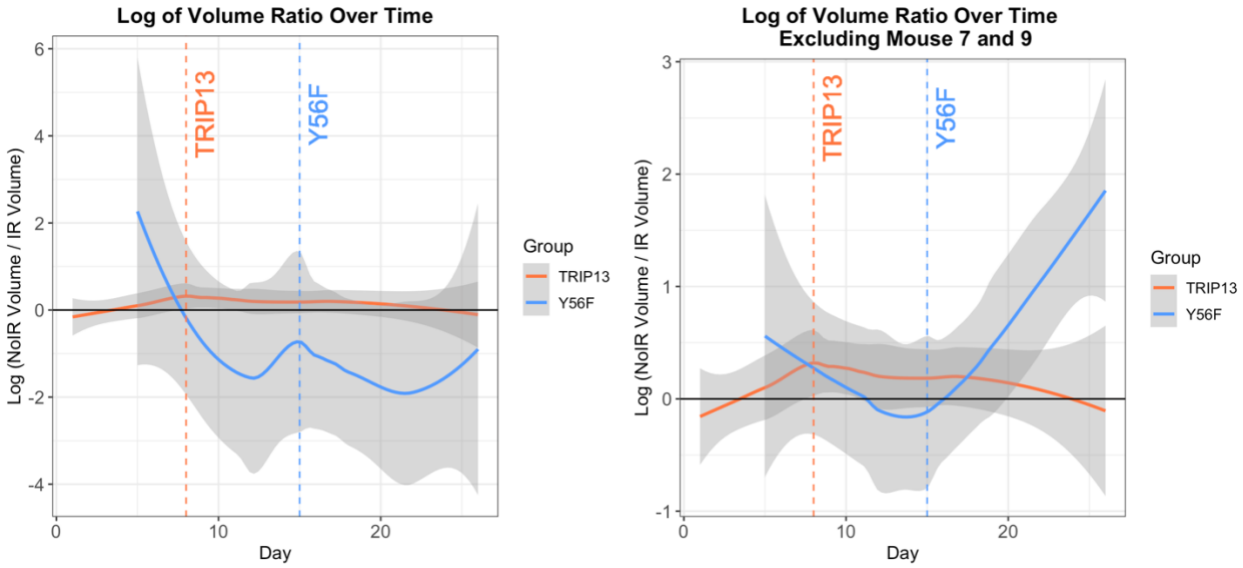

Figure 4: Loess smooth curves of the outcome of the linear mixed effects model, the natural log of the ratio of non-irradiated tumor volume to irradiated tumor volume, over time. Start of radiation for each group is indicated via dashed vertical lines. Plot on the left represents loess smoothed curves from the entire sample. Plot on the right represents loess smoothed curves for the sample excluding mouse 7 and mouse 9.

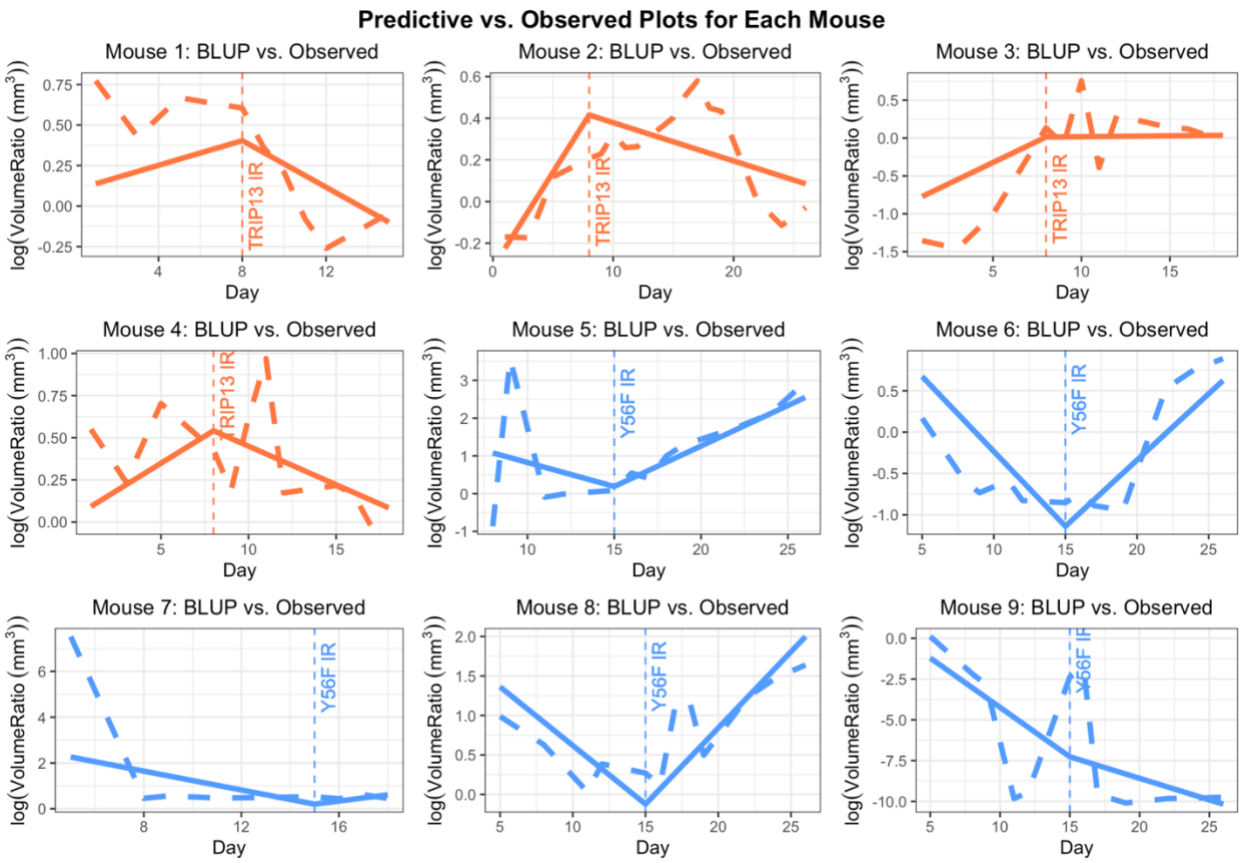

Figure 5: Predicted and observed log volume ratios for all mice in the study. Predicted trajectories are indicated with solid lines and observed trajectories are indicated with dashed lines. Plots of mice in the TRIP13 group are colored in coral and plots of mice in the Y56F group are colored in blue.

Appendix

$$log\left(\frac{VolumeNoIR}{VolumeIR}\right)_{ij} = \beta_0 + \beta_1 Day_{ij} + \beta_2 I(Y56_i = 1) + \beta_3\, Day_{ij} * I(Y56_i = 1) + \beta_4\, I(Y56_i = 0) * (Day_{ij} - 17)_+ + \beta_5\, I(Y56_i = 1) * (Day_{ij} - 24)_+ + b_{0i} + b_{1i} Day_{ij} + \epsilon_{ij}$$

We define the following:

- $log\left(\frac{VolumeNoIR}{VolumeIR}\right)_{ij}$ as the log of tumor volume ratio at the jth day of volume measurement for the ith mouse
- Day_{ij} as the jth day of volume measurement for the ith mouse
- $Y56_{ij}$ as a binary indicator indicating whether or not the ith mouse was assigned to the Y56 group

where $b_{0i} \sim N(0, G)$ and $b_{1i} \sim N(0, G)$ are independent of $\epsilon_{ij} \sim N(0, \sigma_{ij}^2)$

Equation 1: Linear mixed effects model equation

	Log Volume Ratio		
Predictors	*Estimates*	*CI*	*p*
Day	0.07	-0.06 – 0.21	0.283
Y56F Group	2.69	-0.27 – 5.65	0.068
TRIP13 Knot	-0.10	-0.25 – 0.04	0.158
Y56F Knot	0.34	0.20 – 0.48	**<0.001**
Day * Y56F Group	-0.25	-0.44 – -0.07	**0.007**
Random Effects			
σ^2	0.54		
$\tau_{00\ id}$	2.25		
$\tau_{11\ id.Time}$	0.01		
$\varrho_{01\ id}$	-0.95		
ICC	0.53		
N_{id}	8		
Observations	96		
Marginal R^2 / Conditional R^2	0.157 / 0.601		

Supplement 2: Parameter estimates of the linear mixed effects model, fit with REML and excluding all data from mouse 9

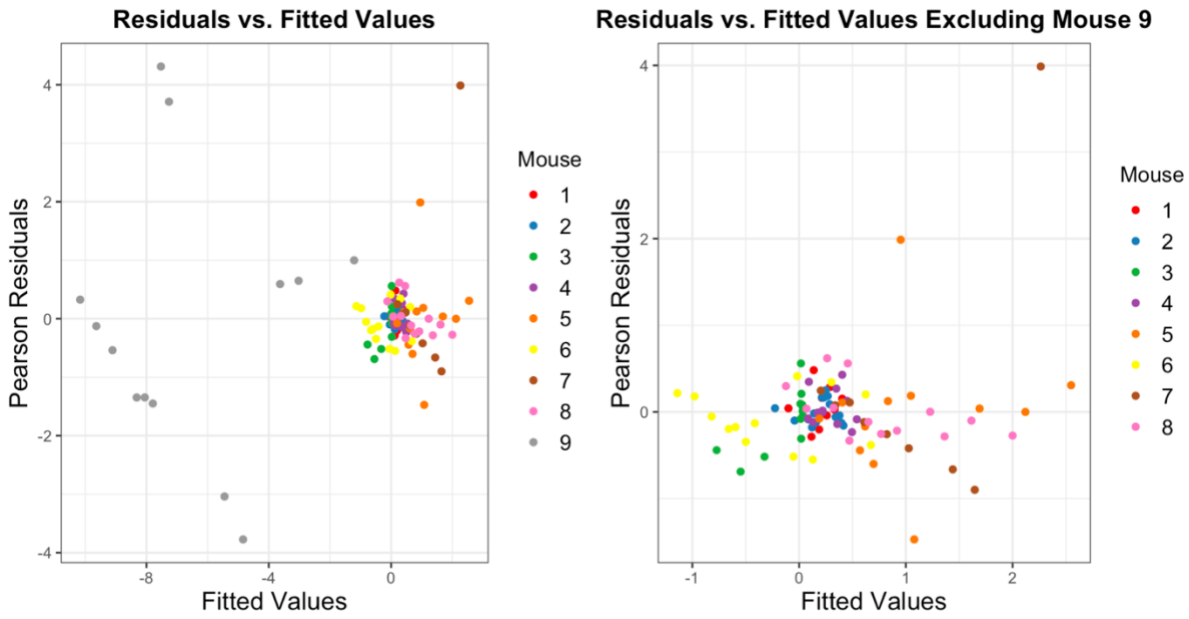

Supplement 3: Plots of residuals vs. fitted values to assess homogeneity of equal variance assumption. The plot on the left represents data from all subjects. For visualization purposes, this same plot was generated without data from mouse 9. Note the change in axis scales between the two plots.

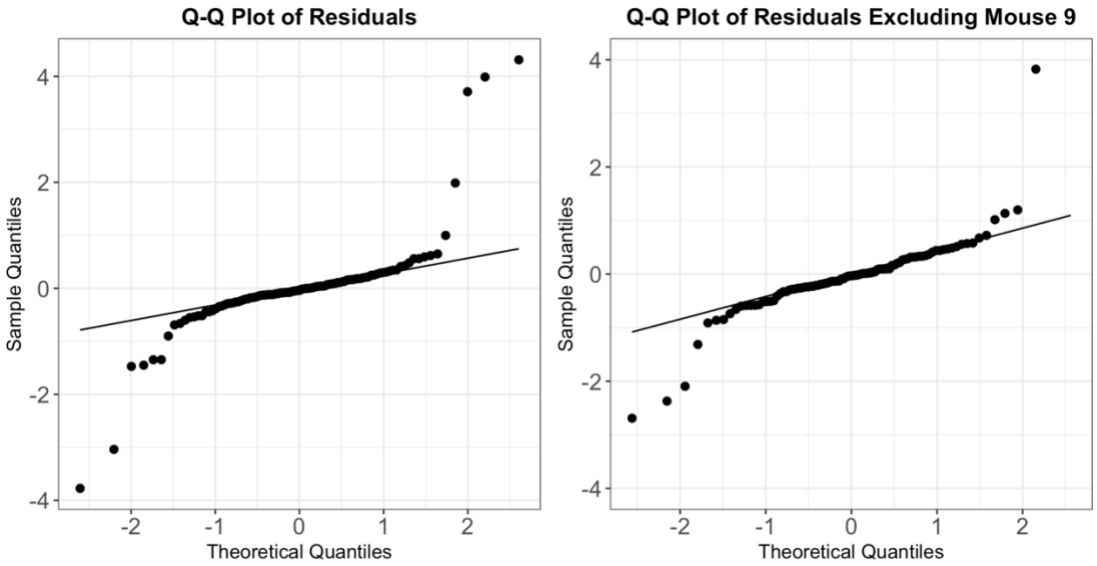

Supplement 4: Quantile-quantile plot of residuals, both with and without data from mouse 9. We see large deviations from normality at the tail ends of the distribution in both plots, indicating non-normal residuals regardless if mouse 9 is included in the analyses.

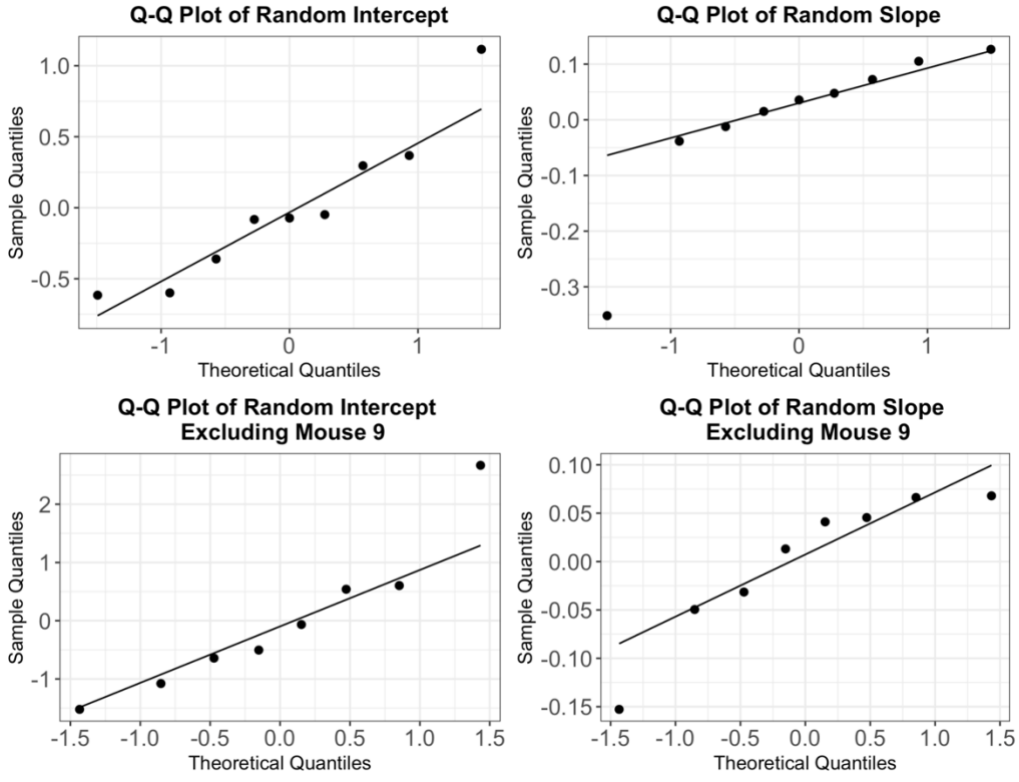

Supplement 5: Quantile-quantile plots of random effects. We see slight deviations from one influential point in both distributions, but removing mouse 9 results in improved normality.

References

Banerjee, R., Liu, M., Bellile, E., Schmitd, L. B., Goto, M., Hutchinson, M.-K. N. D., Singh, P., Zhang, S., Damodaran, D. P. V., Nyati, M. K., Spector, M. E., Ward, B., Wolf, G., Casper, K., Mierzwa, M., & D'Silva, N. J. (2022). Phosphorylation of Trip13 at Y56 induces radiation resistance but sensitizes head and neck cancer to Cetuximab. *Molecular Therapy*, *30*(1), 468–484. https://doi.org/10.1016/j.ymthe.2021.06.009

Johnson, D. E., Burtness, B., Leemans, C. R., Lui, V. W., Bauman, J. E., & Grandis, J. R. (2020). Head and neck squamous cell carcinoma. *Nature Reviews Disease Primers*, *6*(1). https://doi.org/10.1038/s41572-020-00224-3